Available online at www.sciencedirect.com
SCIENCE DIRECT
Journal of the European Ceramic Society 26 (2006) 1237–1244
www.elsevier.com/locate/jeurceramsoc

Microstructures and electrical properties of lead zinc niobate–lead titanate–lead zirconate ceramics using microwave sintering

Chen-Liang Li, Chen-Chia Chou *

Department of Mechanical Engineering, National Taiwan University of Science and Technology, 43 keelong Road, Section 4, Taipei 10672, Taiwan

Received 8 December 2004; received in revised form 1 February 2005; accepted 4 February 2005
Available online 25 April 2005

Abstract

Electrical properties and microstructural characteristics of $(1-x)(0.94PbZn_{1/3}Nb_{2/3}O_3 + 0.06BaTiO_3) + xPbZr_yTi_{1-y}O_3$ (PZN–PZ–PT) ceramics, sintered by microwave heating, were investigated using electron microscopy, energy-dispersive spectroscopy (EDS) and electrical property measurement. Experimental results imply that the microwave-sintered (MW) samples with $x = 0.5$ and $y = 0.52$ (1150 °C, 10 min) possess higher dielectric constant than the conventionally sintered (CS) specimens (1150 °C, 2 h). Microstructural investigations show that ZnO precipitated on the surfaces of specimens during a thermal process, implying that ZnO diffusion may have influenced the distribution of phases in a specimen due to an eutectic reaction of PbO and ZnO. TEM–EDS investigations show that the CS specimens exhibit pronounced elemental segregation of PbO and ZnO at the grain boundaries, but it is much less significant for MW samples. The results imply that microwave sintering not only enhances material densification markedly, but also reduces the PbO/ZnO segregation and amorphous intergranular layers effectively, and thus improve the electrical properties of PZN–PZ–PT ceramics.

Keywords: Microwave processing; Electrical properties; Electron microscopy; PZN–PZ–PT

1. Introduction

Lead zinc niobate, $Pb(Zn_{1/3}Nb_{2/3})O_3$ (PZN), is a relaxor type of ferroelectric material with a partially ordered perovskite structure.[1–3] The PZN has not only very good dielectric properties but also excellent piezoelectric properties.[4–11] However, synthesizing perovskite PZN or $Pb(Zn_{1/3}Nb_{2/3})O_3$–$PbTiO_3$ (PZN–PT) ceramics near morphotropic phase boundary (MPB) using a conventional ceramic process is difficult, because pyrochlore phases form easily.[12–15] Perovskite PZN and 0.9PZN–0.1PT crystals have been reported to be thermodynamically unstable over the wide range of temperatures 600–1400 °C.[13] Lim et al.[14] investigated that the perovskite PZN–PT single crystals decomposed to the pyrochlore phase, PbO and ZnO during high temperature annealing, even in PbO-rich environments. Jang et al.[15] studied the mechanism of formation of perovskite PZN in a molten PbO environment. They also noted that the intermediate pyrochlore phase was zinc-deficient in comparison with perovskite PZN and had a composition of $Pb_{1.83}Zn_{0.29}Nb_{1.71}O_{6.39}$; this formula differs from that noted by earlier researcher ($Pb_3Nb_4O_{13}$).[13] Currently, the most useful method for stabilizing the perovskite structure is to add such additives as $BaTiO_3$ (BT), $SrTiO_3$ (ST) and others.[16,17] The large tolerance factor and ionic nature of the perovskite material are believed to be able to stabilize the PZN perovskite structure.[18] Slight increase of the amount of BT stabilizes PZN.[16,17] However, the phase transformation temperature of PZN may be reduced to lower than the room temperature. Accordingly, other stabilizers must be added to raise the phase transformation temperature of ferroelectric–paraelectric transition and to modify the structure of materials. $PbTiO_3$ (PT) and $PbZrO_3$ (PZ) are therefore commonly employed to adjust those properties.[19,21]

Many investigations have reported the development of high-performance piezoelectric materials such as

* Corresponding author.
E-mail address: cchou@mail.ntust.edu.tw (C.-C. Chou).

0955-2219/$ – see front matter © 2005 Published by Elsevier Ltd.
doi:10.1016/j.jeurceramsoc.2005.02.001

$Pb(Zr,Ti)O_3$ (PZT), $PbLa(Zr,Ti)O_3$ (PLZT) using microwave sintering.[22–31] The 2.45 and 30 GHz microwave were used in sintering of PZT ceramics, whose property was improved because of reducing the PbO volatility.[28,29] However, the electrical characteristics of MW samples was reported to be similar to or inferior to those of the CS samples with the same specimen density, if the MW sintering was carried out at a temperature lower than that of a CS process over 100 °C.[32] The reason for this was attributed to the crystallinity, grain size, and domain structure development in materials.[32]

To elucidate microstructural development of the PbO and ZnO containing materials using MW, we employed $BaTiO_3$ to stabilize PZN and used PT and PZ to control the phase structure and electrical characteristics of PZN-based materials in this work. Besides, electrical and microstructural characteristics of the specimens sintered using microwave sintering were compared to those of the CS samples. The feasibility of using microwaves to fabricate PZN-based ceramics is evaluated and an attempt is made to clarify the mechanisms of improvements of the electrical properties of PZN–PZ–PT ceramics.

2. Experimental procedures

Nominal composition of the specimens of $x(0.94PbZn_{1/3}Nb_{2/3}O_3 + 0.06BaTiO_3) + (1-x)PbZr_yTi_{1-y}O_3$ (PZN–PZ–PT) was fabricated, and specimens with $x = 0.5$ and $y = 0.52$ exhibited acceptable dielectric and piezoelectric properties, and therefore was investigated in this experiment. The results obtained with other compositions have been and will be reported elsewhere.[33,34] BT, PT and PZ is used herein to stabilize perovskite PZN and employed to modify the desired phase and electrical characteristics. The specimens were prepared by an A-site-element sequential mixing columbite (ASMC) method.[33,34] Following calcinations, the ground and ball-milled powders were pressed into discs with a diameter of 10 mm and a thickness of 1 mm using a pressure of 120 MPa. A multimode 2.45 GHz microwave furnace with a power output of 1 kW was used in the microwave sintering process, and the specimens were sintered at various temperatures from 10 to 120 min. The conventionally sintering (CS) process was performed at 1150 °C for 2 h using a double crucible that contained $PbZrO_3$ powders to prevent the evaporation of PbO. Fig. 1 displays the experimental set-up of the MW process and temperature profiles of the MW and the CS processes. The phase structures of the powders and the disc specimens were analyzed using an X-ray diffractometer with Cu Kα radiation. After the specimens had been polished to a thickness of 0.6 mm, a silver paste was applied as the electrodes and baked at 600 °C for 30 min to enable electrical measurements to be made. The dependence of the dielectric constant on temperature of specimens was measured from 100 Hz to 1 MHz using a gain-phase analyzer (HP 4194A) with an automatic temperature-controlled chamber in the temperature range of 25–400 °C. The samples were poled by applying a dc field of 5 kV/mm at 100 °C for 30 min. The

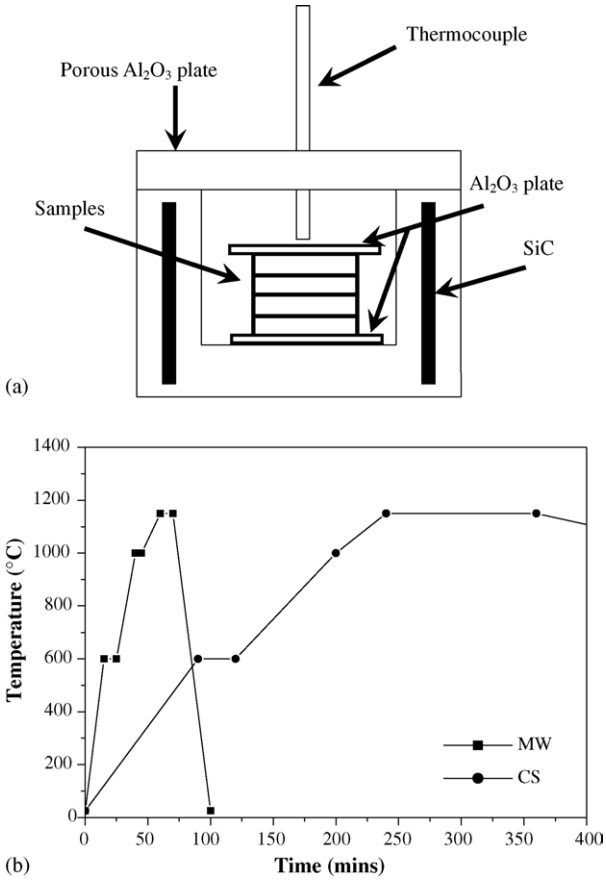

Fig. 1. (a) Experimental set-up for MW process and (b) sintering temperature profiles of the CS and the MW processes.

piezoelectric planar coupling coefficient (k_p) was determined by the resonance–antiresonance method using a HP 4194A. The electromechanical coupling coefficient k_p was calculated by $k_p = \sqrt{2.51[(f_a - f_r)/f_r]}$ (f_a is the antiresonant frequency and f_r is the resonant frequency). The chemical homogeneity of the specimens was investigated using an energy-dispersive X-ray spectrometer (EDS) on a transmission electron microscope with a field emission gun (FEG-TEM) (Philips Tecnai F30) with an EDS system and an FEG scanning electron microscope (FEG-SEM) (JEOL 6500F). The electron beam was converged to 10 nm during the EDS investigations using the FEG-TEM. Scanning electron micrographs of the fractured surface and grain morphology were obtained to evaluate the grain size and surface characteristics.

3. Results and discussion

Fabrication of specimens using microwave exhibits much faster densification rate than using a conventional sintering process. Fig. 2 plots the relative density and the grain size of PZN–PZ–PT specimens sintered using the MW process. The relative density of specimens reached 95% when the sintering was carried out at 1050 °C for 10 min, implying that the material rapidly absorbed microwave energy and become den-

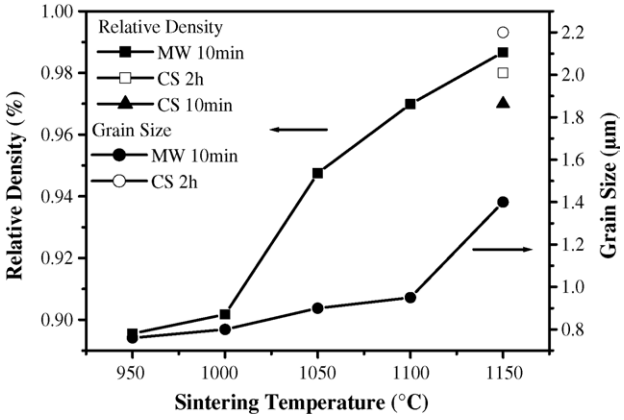

Fig. 2. Relative densities and grain sizes of PZN–PZ–PT specimens sintered by the MW and CS process at various sintering temperature and soaking time.

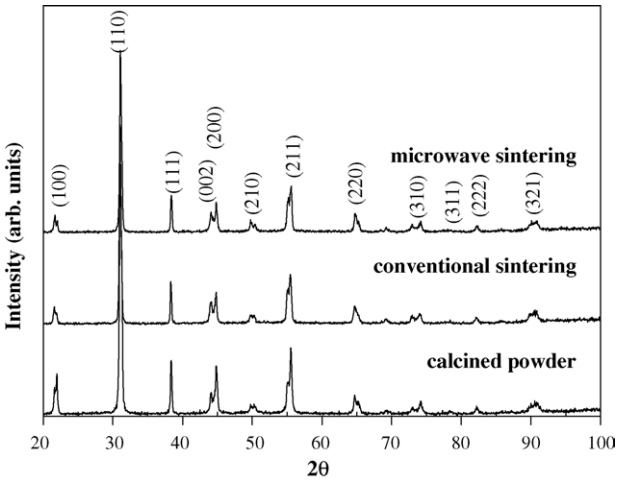

Fig. 3. XRD patterns of PZN–PZ–PT powder calcined at 950 °C for 4 h and specimens sintered at 1150 °C for 2 h and 10 min by CS and MW processes, respectively.

sified. The relative density of the MW samples could reach 98% at a sintering temperature of 1150 °C for 10 min. On the other hand, using a CS process to achieve relative density of samples of 98% required a processing time of 2 h at 1150 °C and must be under a strict atmospheric control. However, thermal runaway would take place at 1150 °C for processing over 15 min in a microwave sintering process. The grains grew quickly when the sintering temperature exceeded 1100 °C during the MW process. The results imply that the samples absorbed microwave energy efficiently, and that different grain growth mechanisms (interface-controlled and diffusion-controlled) may operate at low and high (>1100 °C) temperatures, respectively. Notably, the grain size of MW samples was always smaller than those of CS samples when the sintering temperature was similar. The grain size of MW and CS samples was 1.4 and 2.2 μm at a sintering temperature of 1150 °C for 10 min and 2 h, respectively.

The pyrochlore phase was very easily formed in the PZN material system. The processing conditions must be chosen carefully to prevent its formation. Fig. 3 displays the XRD patterns of the microwave and conventionally sintered PZN–PZ–PT ceramics generated from powders using an ASMC method, which effectively reduces pyrochlore phase generation.[33,34] The significance of the ASMC method is that we not only mix B-site elements in advance, but also consider the A-site element activity and therefore addition sequence of the elements. Specimens with complete perovskite phase can be obtained at the current composition sintered by the MW process at 1150 °C for 10 min and the CS process for 2 h. Notably, the CS process was carried out in a PbO-rich atmosphere, but preventing the loss of PbO from the specimen surface layer during processing was still difficult. On the other hand, the MW sintering process was performed in an Al_2O_3 container covered with insulation pad with less atmosphere protection and samples without forming the pyrochlore phase were produced.

The dielectric constants of both MW (1150 °C, 10 min) and CS (1150 °C, 2 h) specimens were evaluated and the results were compared. The dielectric constants and dielectric loss were measured as a function of temperature, *K–T*, at 1 kHz at a range of temperatures from 25 to 400 °C, as shown in Fig. 4. The maximum dielectric constant, K_{max}, was 16,000 for the MW specimens, but approximately 14,000 for the CS specimens. Samples that have undergone the microwave process have a dielectric constant that is 14% higher than those of conventionally sintered specimens. More interestingly, the dielectric loss of MW specimens at Curie temperature (T_c) temperature was only about 1/4 of that of CS ones. The T_c of the specimens that underwent microwave sintering was approximately 10 °C lower, giving an indication hint of microstructural difference between MW and CS samples.

Fig. 5 shows the impedance spectra of the MW and the CS specimens. The first resonant and antiresonant frequencies of the MW samples were at 246 and 281 kHz, respectively. For CS samples the impedance peak of resonant and antiresonant frequency appears at 250 and 280 kHz, respectively. The MW

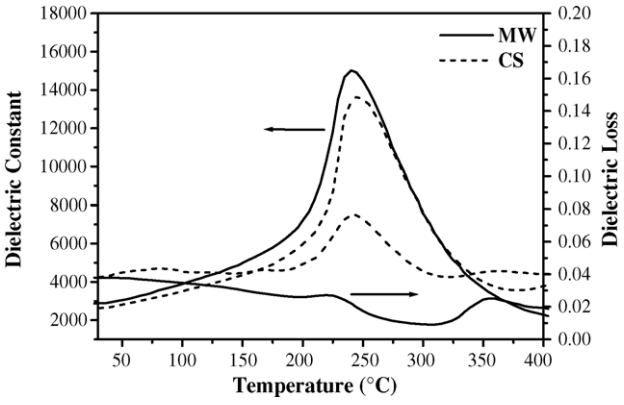

Fig. 4. Temperature-dependent relative dielectric permittivity and dielectric loss of PZN–PZ–PT at 1 kHz for CS and MW samples. Specimens were sintering at 1150 °C for 2 h and 10 min by the CS and the MW processes, respectively.

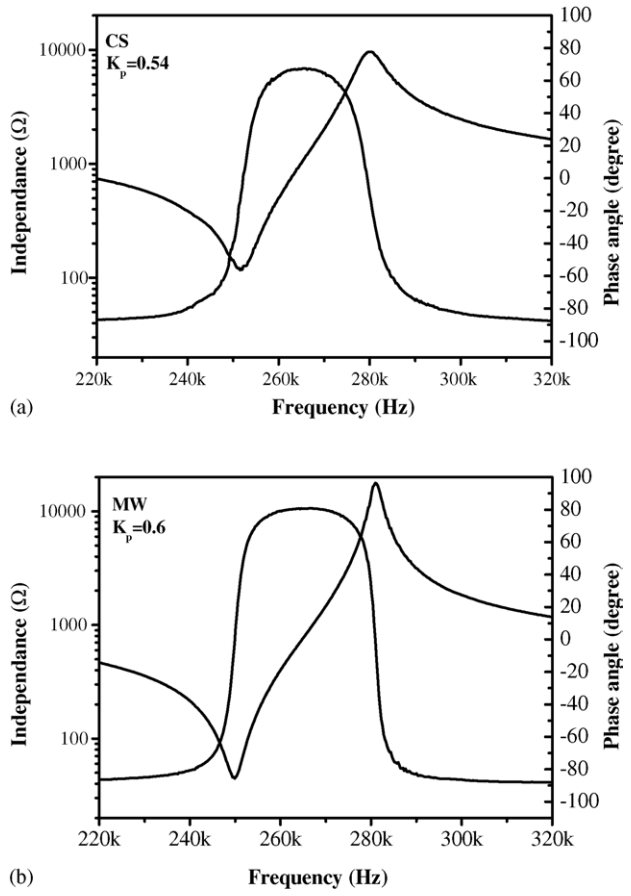

Fig. 5. Resonance curves and phase angle obtained through the piezoelectric characterization for the (a) CS and (b) MW processed PZN–PZ–PT specimens.

specimen exhibits a wider frequency of difference between f_a and f_r, and a more square shape of the impedance curve. It was shown that the magnitude of k_p of MW samples was higher ($k_p = 0.6$ for MW and 0.54 for CS). On the other hand, the resonant impedance of MW samples was lower than those of CS samples, suggesting that MW samples possess less defects or better crystallinity. The lower resonant impedance implies that specimens exhibit higher mechanical quality factor and lower heat dissipation during working.

The experiments performed in this work revealed some re-deposited or diffused-out particulates on the surface of the specimens, under thermal etching at 1000 °C for 30 min, as shown in Fig. 6. Table 1 shows the semi-quantitative EDS analysis. The particulates consisted of primarily ZnO (~40.74 at.%) and PbO (~41.36 at.%), which implies that

Table 1
SEM–EDS elemental analysis of the re-precipitation particles on surface of PZN–PZ–PT specimen after thermal etching

	Element					
	Ti	Zn	Zr	Nb	Ba	Pb
Weight%	1.28	20.06	1.48	5.79	4.55	66.29
Atomic%	3.47	40.74	2.1	8.05	4.28	41.36

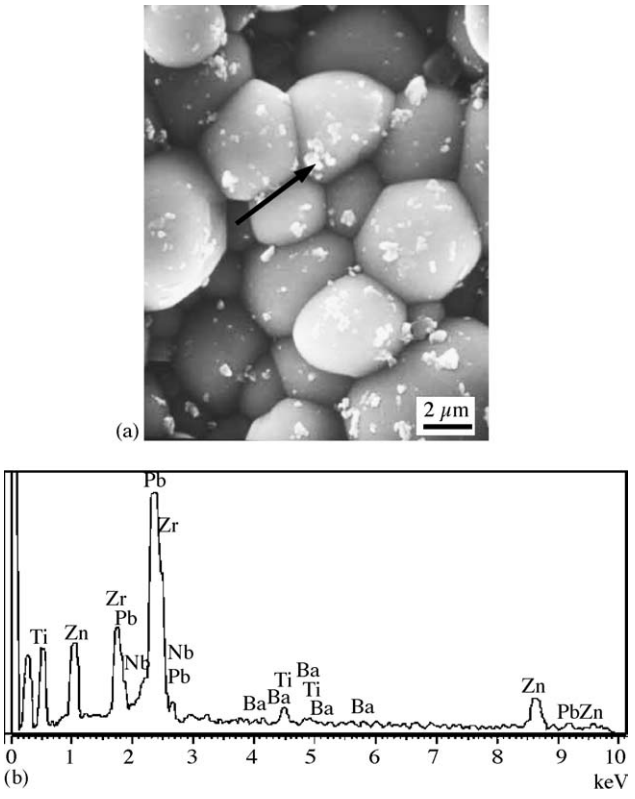

Fig. 6. An SEM micrograph of CS samples showing some re-precipitation particles existing on specimen surface after thermal etching. (a) SEM image and (b) EDS spectrum.

the zinc oxide is easily decomposed during material processing. Intriguingly, ZnO exhibits vapor pressure two orders lower than PbO. Enhancement of the ZnO diffusion may be attributed to the eutectic reaction of ZnO and PbO at around 860 °C. ZnO was extracted out from grains to the surface and form the liquid phase. However, PbO keeps evaporating and leaves high concentration of ZnO in the liquid phase. After cooling down, the particulates form on specimen surface. The consequence of PbO evaporation and ZnO diffusing-out is the formation of the pyrochlore phase or degradation of dielectric properties of the grains.

TEM investigations were also performed to investigate the microstructural characteristics of the specimens. Under as-sintered conditions, both CS and MW specimens display simple and similar grain interior which is different from the specimens microwave-sintered at lower temperatures, which exhibit complicated domain arrangements in materials.[32] Fig. 7 displays the atomic structure images of grain boundaries in PZN–PZ–PT specimens using the CS and MW processes. The CS specimen exhibits uniform grains, but possesses obviously an amorphous phase among grains. On the other hand, the MW specimen does not obviously exhibit such a grain boundary layer. It was reported that PbO might segregate to form the amorphous layer or second phases.[35–37] Fig. 8 and Table 2 display the corresponding EDS spectra of the

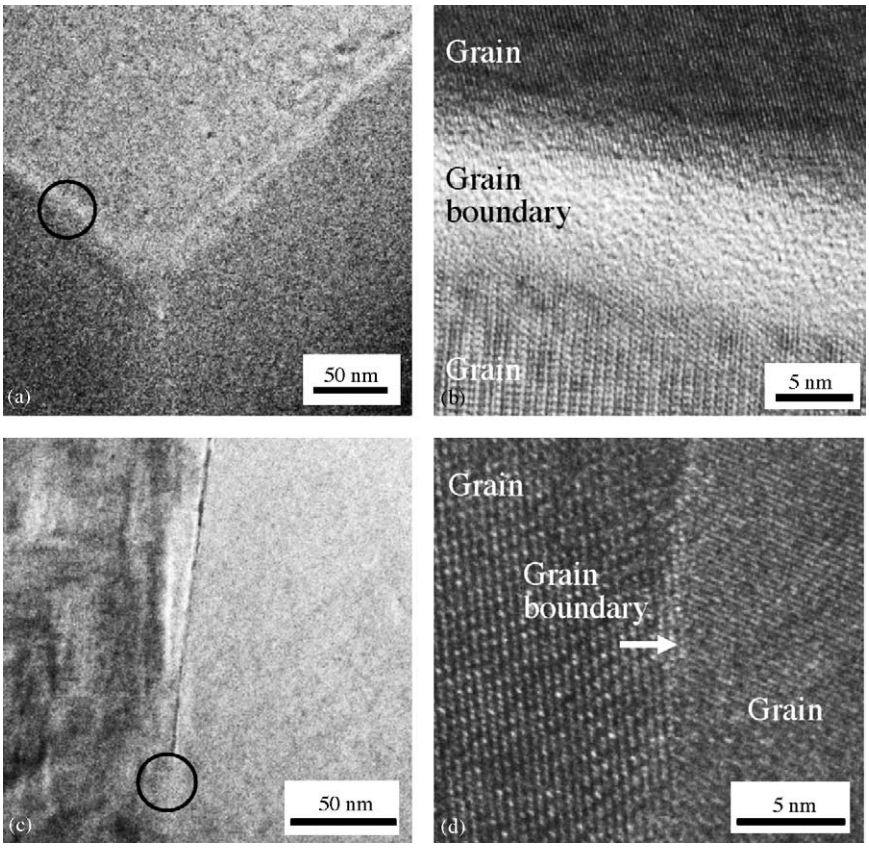

Fig. 7. Atomic structure images of grain boundaries in PZN–PZ–PT specimens using the (a and b) CS and (c and d) MW processes.

CS and MW specimens. A semi-quantitative EDS study of the grain boundary showed that the grain boundaries of the CS samples possess more PbO and ZnO, but the MW samples do not exhibit extraordinary concentration gradient due to insignificant existence of the inter-grain-boundary layer. Therefore, at the current material system, not only PbO but also ZnO forming the intergranular layer of a thickness of about 10 nm, which may have a lower dielectric constant, surrounds grains of higher dielectric constant as shown in Figs. 7(a, b) and 8(a). The dielectric constant declines as the amount of the grain boundary layer with lower dielectric constant increases. However, the MW process can suppress PbO and ZnO losses and reduce the annealing time. Figs. 7(c, d) and 8(b) shows the grain boundaries of MW samples at a sintering time of 10 min. The micrograph displays a clear grain boundary with thickness less than 1 nm.

Table 2
TEM–EDS elemental analyses of grain boundaries for MW and CS PZN–PZ–PT samples (unit: at.%)

Element	CS	MW
Ti	7.21	15.59
Zn	44.56	7.95
Zr	1.85	12.75
Nb	1.6	16.12
Pb	44.78	47.6

The composition analysis at the grain boundary is also similar to that of grain interior. If microwave sintering proceeds longer, thicker intergranular layer may form, but the segregation is not as significant as that in CS specimens. The results suggest that the volatile elements such as PbO and ZnO segregating to grain boundaries are much less pronounced in the MW process, which produces better crystallinity and fewer defects in materials.

Lim et al.[14] investigated that the perovskite PZN–PT single crystals decomposed to the pyrochlore phase, PbO and ZnO during high temperature annealing, even in PbO-rich environments. Jang et al.[15] studied the mechanism of formation of perovskite PZN in a molten PbO environment and noted that, in comparison with perovskite PZN, the intermediate pyrochlore phase was zinc-deficient. Using the PbO atmosphere in the CS process can suppress PbO and ZnO evaporation from the surface of the samples, but it did not prevent segregation of PbO and ZnO inside the sample along grain boundaries. Furthermore, there was an eutectic point in PbO and ZnO binary system at a composition of 15 mol% ZnO at 860 °C.[38] When PbO and ZnO segregate at grain boundaries during the sintering process, a liquid phase occurs and the diffusion rate increases. This may be the reason why PZN-based materials can be sintered at lower temperatures, and the CS samples exhibit a thick amorphous layer at grain boundaries as well.

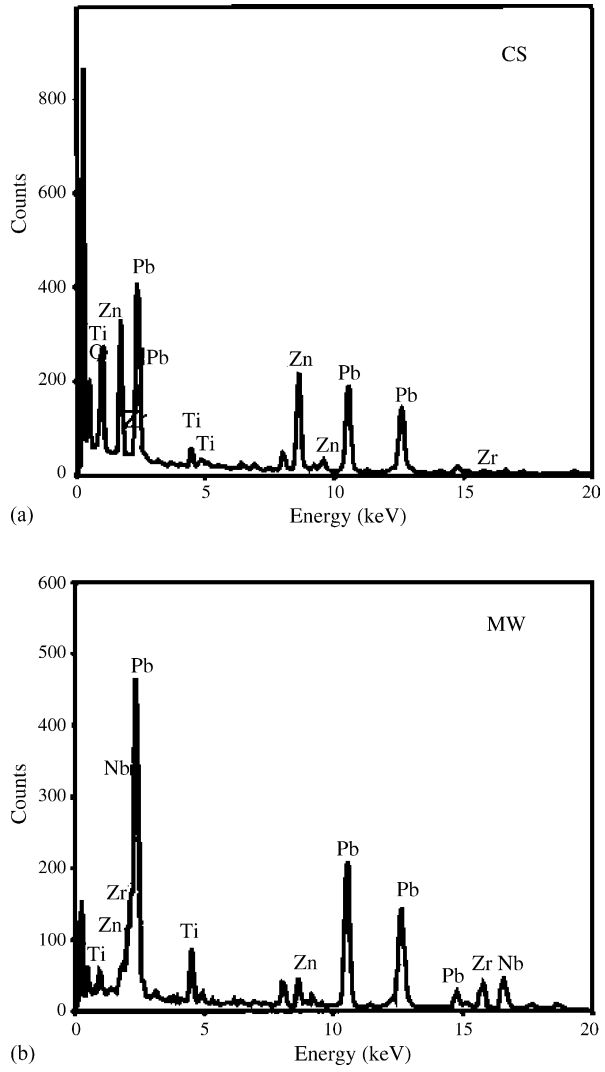

Fig. 8. EDS spectra of a grain boundary in PZN–PZ–PT specimens using a (a) CS and (b) MW processes.

For Pb-based systems with excess PbO, the possibility of the existence of a low-permittivity intergranular phase was suggested and examined using the series mixing model.[20,37] According to the series mixing model of diphasic systems,[39] the relative dielectric permittivity of polycrystalline ceramics is given by

$$\frac{D}{\varepsilon_s} = \frac{D_g}{\varepsilon_g} + \frac{D_{gb}}{\varepsilon_{gb}}$$

where ε_s is the relative dielectric permittivity of the specimen; ε_g is the inherent dielectric permittivity of the perovskite grain, excluding the grain-boundary region; ε_{gb} is that of the grain-boundary phase; D_g is the thickness of the grain core; D_{gb} is that of the grain-boundary region; and D is the total thickness of the grain. Because the thickness of the grain boundary phase is so small in MW samples, we assume that dielectric constant of MW samples is equal to its grain dielectric constant. We further assume that the dielectric constant of the grain in CS samples is the same as that of MW ones. Consequently, we can estimate the grain boundary dielectric constant of CS samples to be about 480. However, Papet et al.[40] find that dielectric constant of the grain boundary phase for PMN is only 20. This result suggests that the segregated ZnO in grain boundary could improve the dielectric constant of the grain boundary phase. We expect the present grain boundary phase possesses lower dielectric constant than the crystalline ZnO ($\varepsilon = 1000$),[41] because it may contain nanocrystalline or amorphous phase at the grain boundaries. Segregation of PbO and ZnO could reduce the dielectric constant of the specimens. However, the dielectric constant of CS sample does not clearly decrease. This result indicates that higher dielectric constant of the grain boundary phase may not be that detrimental to dielectric properties in PZN-base materials, comparing with other lead-based systems with excess lead oxide addition.[35,36,42]

More importantly, microwave sintering reduces the PbO/ZnO evaporation and segregation effectively, and therefore greatly enhances reliability of the material processing and material properties. The results imply potential applications of microwave sintering in future devices and materials processing for material systems with high vapor pressure.

4. Conclusions

The relationship between microstructures and electrical properties of PZN–PZ–PT ceramics is investigated using MW and CS processes. The experimental results show that the relative density of the MW samples achieve 98% at the sintering temperature of 1150 °C for 10 min, similar to that of CS samples at 1150 °C for 2 h. The dielectric constant of the MW samples was 14% higher than those of the CS samples and dielectric loss was much less than that of CS ones. Grain size in the MW specimens was much smaller than that in the CS process at the same density with the same sintering temperature. However, the smaller grain size did not degrade the electrical properties of MW specimens. SEM investigations showed that ZnO may precipitate or redeposit on the surface of the specimens during the thermal process. Transmission electron micrographs indicate that the as-sintered MW samples exhibit very simple grain interior similar to those of the CS samples. However, high resolution TEM and energy-dispersive spectroscopic investigations show that the grain boundaries of MW samples contain much less PbO and ZnO segregation than those of the CS samples. These findings indicate that the MW process can reduce the total thickness of PbO-rich and ZnO-rich amorphous intergranular layers significantly, and thus improve the electrical properties of PZN–PZ–PT ceramics.

Acknowledgments

Financial support from the National Science Council of Taiwan, Republic of China through project numbers NSC

90-2216-E-011-044 and NSC 91-2216-E-011-031 is gratefully acknowledged by the authors. C.C.C. would also like to express his appreciation to Sinetek Co. Ltd. of Taiwan for providing excellent conductive pastes.

References

1. Kuwata, J., Uchino, K. and Nomura, S., Diffuse phase transition in lead zinc niobate. *Ferroelectrics*, 1979, **22**, 863–867.
2. Rajan, K. K. and Lim, L. C., Particle size dependent X-ray linewidth of rhombohedral phase in $Pb(Zn_{1/3}Nb_{2/3})O_3$–(6,7)%$PbTiO_3$. *Appl. Phys. Lett.*, 2003, **83**, 5277–5279.
3. Lu, Y., Jeong, D. Y., Cheng, Z. Y., Shrout, T. and Zhang, Q. M., Phase stabilities of "morphotropic" phases in $Pb(Zn_{1/3}Nb_{2/3})O_3$–$PbTiO_3$ single crystals. *Appl. Phys. Lett.*, 2002, **80**, 1918–1920.
4. Park, S. E. and Shrout, T. R., Ultrahigh strain and piezoelectric behavior in relaxor based ferroelectric single crystals. *J. Appl. Phys.*, 1997, **82**, 1804–1811.
5. Liu, S. F., Park, S. E., Shrout, T. R. and Cross, L. E., Electric field dependence of piezoelectric properties for rhombohedral $0.955Pb(Zn_{1/3}Nb_{2/3})O_3$–$0.045PbTiO_3$ single crystals. *J. Appl. Phys.*, 1999, **85**, 2810–2814.
6. Paik, D. S., Park, S. E., Wada, S., Liu, S. F. and Shrout, T. R., *E*-field induced phase transition in ⟨0 0 1⟩-oriented rhombohedral $0.92Pb(Zn_{1/3}Nb_{2/3})O_3$–$0.08PbTiO_3$ crystals. *J. Appl. Phys.*, 1999, **85**, 1080–1083.
7. Ren, W., Liu, S. F. and Mukherjee, B. K., Nonlinear behavior of piezoelectric lead zinc niobate–lead titanate single crystals under ac electric fields and dc bias. *Appl. Phys. Lett.*, 2003, **83**, 5268–5270.
8. Liu, S. F., Ren, W., Mukherjee, B. K., Zhang, S. J., Shrout, T. R., Rehrig, P. W. *et al.*, The piezoelectric shear strain coefficient of ⟨1 1 1⟩-oriented $Pb(Zn_{1/3}Nb_{2/3})O_3$–$PbTiO_3$ piezocrystals. *Appl. Phys. Lett.*, 2003, **83**, 2886–2888.
9. Ko, J. H., Kim, D. H. and Kojima, S., Elastic responses to different electric-field directions in relaxor ferroelectric $Pb[(Zn_{1/3}Nb_{2/3})_{0.91}Ti_{0.09}]O_3$ single crystals. *Appl. Phys. Lett.*, 2003, **83**, 2037–2039.
10. Barad, Y., Lu, Y., Cheng, Z. Y., Park, S. E. and Zhang, Q. M., Composition, temperature, and crystal orientation dependence of the linear electro-optic properties of $Pb(Zn_{1/3}Nb_{2/3})O_3$–$PbTiO_3$ single crystals. *Appl. Phys. Lett.*, 2000, **77**, 1247–1249.
11. Yin, J. and Cao, W., Coercive field of $0.955Pb(Zn_{1/3}Nb_{2/3})O_3$–$0.045PbTiO_3$ single crystal and its frequency dependence. *Appl. Phys. Lett.*, 2002, **80**, 1043–1045.
12. Kuwata, J., Uchino, K. and Nomura, S., Phase transitions in the $Pb(Zn_{1/3}Nb_{2/3})O_3$–$PbTiO_3$ system. *Ferroelectric*, 1981, **37**, 579–582.
13. Chen, S. Y., Wang, C. M. and Cheng, S. Y., Role of perovskite PMN in phase formation and electrical properties of high dielectric $Pb[(Mg_x,Zn_{1-x})_{1/3}Nb_{2/3}]O_3$ ceramics. *Mater. Chem. Phys.*, 1998, **52**, 207–213.
14. Lim, L. C., Liu, R. and Kumar, F. J., Surface breakaway decomposition of perovskite 0.91PZN–0.09PT during high-temperature annealing. *J. Am. Ceram. Soc.*, 2002, **85**, 2817–2826.
15. Jang, H. M., Oh, S. H. and Moon, J. H., Thermodynamic stability and mechanisms of formation and decomposition of perovskite $Pb(Zn_{1/3}Nb_{2/3})O_3$ prepared by the PbO flux method. *J. Am. Ceram. Soc.*, 1992, **75**, 82–88.
16. Halliyal, A., Kumar, U., Newnham, R. E. and Cross, L. E., Dielectric and ferroelectric properties of ceramics in the $Pb(Zn_{1/3}Nb_{2/3})O_3$–$BaTiO_3$–$PbTiO_3$. *J. Am. Ceram. Soc.*, 1987, **70**, 119–124.
17. Belsick, J. R., Halliyal, A., Kumar, U. and Newnham, R. E., Phase relations and dielectric properties of ceramics in the system $Pb(Zn_{1/3}Nb_{2/3})O_3$–$SrTiO_3$–$PbTiO_3$. *Am. Ceram. Soc. Bull.*, 1987, **66**, 664–667.
18. Zhu, W., Kholkin, A. L., Mantas, P. Q. and Baptista, J. L., Morphotropic phase boundary in the $Pb(Zn_{1/3}Nb_{2/3}O_3)$–$BaTiO_3$–$PbTiO_3$ system. *J. Am. Ceram. Soc.*, 2001, **84**, 1740–1744.
19. Kumar, U., Cross, L. E. and Halliyal, A., Pyroelectric and electrostrictive properties of $(1-x-y)$PZN·xBT·yPT ceramic solid solutions. *J. Am. Ceram. Soc.*, 1992, **75**, 2155–2164.
20. Wi, S. K. and Kim, H. G., Domain reorientation effects on the temperature dependence of piezoelectric properties in $Pb(Zn_{1/3}Nb_{2/3})O_3$–$PbZrO_3$–$PbTiO_3$ ceramics. *Jpn. J. Appl. Phys.*, 1992, **31**, 2825–2828.
21. Cho, Y. S., Pilgrim, S. M., Giesche, H. and Bridger, K., Dielectric and electromechanical properties of chemically modified PMN–PT–BT ceramics. *J. Am. Ceram. Soc.*, 2000, **83**, 2473–2480.
22. Xie, Z., Yang, J., Huang, X. and Huang, Y., Microwave processing and properties of ceramics with different dielectric loss. *J. Eur. Ceram. Soc.*, 1999, **19**, 381–387.
23. Goldstein, A. and Kravchik, M., Sintering of PZT powders in MW furnace at 2.45 GHz. *J. Eur. Ceram. Soc.*, 1999, **19**, 989–992.
24. Harrison, W. B., Hanson, M. R. B. and Koepke, B. G., Microwave processing and sintering of PZT and PLZT ceramics. *Mater. Res. Soc. Symp. Proc.*, 1988, **124**, 279–286.
25. Takahashi, H., Kato, K., Jinhao, Q. and Junji, T., Property of lead zirconate titanate actuator manufactured with microwave sintering process. *Jpn. J. Appl. Phys.*, 2001, **40**, 724–727.
26. Hu, C. T., Chen, H. W., Chang, H. Y. and Lin, I. N., Effect of SiO_2 sintering aids on high critical temperature positive temperature coefficient of resistivity properties of $(Pb_{0.6}Sr_{0.3}Ba_{0.1})TiO_3$ materials prepared by microwave sintering technique. *Jpn. J. Appl. Phys.*, 1998, **37**, 186–191.
27. Xie, Z., Gui, Z., Li, L., Su, T. and Huang, Y., Microwave sintering of lead-based relaxor ferroelectric ceramics. *Mater. Lett.*, 1998, **36**, 191–194.
28. Rhee, S., Agrawal, D., Shrout, T. and Thumm, M., Investigation of high microwave frequency (2.45 GHz, 30 GHz) sintering for Pb-based ferroelectrics and microscale functional devices. *Ferroelectrics*, 2001, **261**, 15–20.
29. Rhee, S., Shrout, T. R., Ritter, T. A. and Thumm, M., Investigation of high frequency (2.45 GHz, 30 GHz) processing of Pb-based piezoelectrics for ultrasound transducers. *IEEE Ultrason. Symp.*, 2000, **2**, 981–984.
30. Chou, C. C., Chen, P. H. and Lin, I. N., Microstructural characteristics of microwave sintered semi-conductive $Pb_{0.6}Sr_{0.4}TiO_3$ ceramics. *Ferroelectrics*, 1999, **231**, 37–42.
31. Chen, P. H., Pan, H. C., Chou, C. C. and Lin, I. N., Microstructures and properties of semiconductive $(Pb_{0.6}Sr_{0.4})TiO_3$ ceramics using $PbTiO_3$-coated $SrTiO_3$ powders. *J. Eur. Ceram. Soc.*, 2001, **21**, 1905–1908.
32. Chou, C. C., Chang, H. Y., Lin, I. N., Shaw, B. J. and Tan, J. T., Microscopic examination of the microwave sintered $(Pb_{0.6}Sr_{0.4})TiO_3$ positive-temperature-coefficient resistor materials. *Jpn. J. Appl. Phys.*, 1998, **37**, 5269–5272.
33. Li, C. L. and Chou, C. C., Electrical properties and microstructures of microwave sintered PZN-based ceramics. *Integr. Ferroelectr.*, 2003, **55**, 955–964.
34. Li, C. L. and Chou, C. C., Preparation of PZN-based ceramics using a sequential mixing columbite method. *Integr. Ferroelectr.*, 2002, **50**, 1549–1558.
35. Song, B. M., Kim, D. Y., Shirasaki, S. I. and Yamamura, H., Effect of excess PbO on the densification of PLZT ceramics. *J. Am. Ceram. Soc.*, 1989, **72**, 833–836.
36. Jang, H. M. and Lee, K. M., Stabilization of $Pb(ZnMg)_{1/3}Nb_{2/3}O_3$–$0.045PbTiO_3$ perovskite phase and dielectric properties of ceramics prepared by excess constituent oxides. *J. Mater. Res.*, 1994, **9**, 2634–2644.

37. Villegas, M., Fernandez, J. F., Caballero, A. C., Samardija, Z., Drazic, G. and Kosec, M., Effects of PbO excess in $Pb(Mg_{1/3}Nb_{2/3})O_3$–$PbTiO_3$ ceramics: Part II. Microstructure development. *J. Mater. Res.*, 1999, **14**, 898–905.
38. Buchanan, R. C., *Ceramic Materials for Electronics*. Marcel Dekker, INC, New York, Basel, Hong Kong, 1991, pp. 360–363.
39. Wang, H. C. and Schulze, W. A., The role of excess magnesium oxide or lead oxide in determining the microstructure and properties of lead magnesium niobate. *J. Am. Ceram. Soc.*, 1990, **73**, 825–832.
40. Papet, P., Dougherty, J. P. and Shrout, T. R., Particle and grain size effects on the dielectric behavior of the relaxor ferroelectric $Pb(Mg_{1/3}Nb_{2/3})O_3$–$PbTiO_3$. *J. Mater. Res.*, 1990, **5**, 2902–2909.
41. Levinson, L. M. and Philipp, H. R., AC properties of metal-oxide varistors. *J. Appl. Phys.*, 1976, **47**, 1117–1122.
42. Jang, H. M. and Lee, K. M., Dielectric and piezoelectric properties of the thermally annealed $Pb(Zn_{1/3}Mg)Nb_{2/3}O_3$–$PbTiO_3$ system across the rhombohedral/tetragonal morphotropic phase boundary. *J. Mater. Res.*, 1995, **10**, 3185–3193.